CRYSTAL GROWTH & DESIGN

pubs.acs.org/crystal

Article

Cocrystallization of Curcuminoids with Hydroxybenzenes Pyrogallol and Hydroxyquinol: Investigations of Binary Thermal Phase Behaviors

Published as part of a Crystal Growth and Design virtual special issue in Celebration of the Career of Roger Davey

Steffi Wünsche, Andreas Seidel-Morgenstern, and Heike Lorenz*

Cite This: *Cryst. Growth Des.* 2022, 22, 3303−3310

Read Online

ACCESS | Metrics & More | Article Recommendations | Supporting Information

ABSTRACT: The binary thermal phase behaviors of the curcuminoids (CURDs) curcumin (CUR), demethoxycurcumin (DMC), and bis-(demethoxy)curcumin (BDMC) with either pyrogallol (PYR) and hydroxyquinol (HYQ) as potential cocrystal formers were investigated. Earlier, it was reported that CUR and BDMC form cocrystals in a 1:1 stoichiometric ratio with the aforementioned coformers. Here, we report for the first time cocrystallization experiments of DMC. Two different cocrystallization techniques, namely, liquid-assisted grinding and cocrystallization from the melt phase, were applied. Analyses of the cocrystallization outcomes were performed using powder X-ray diffraction and differential scanning calorimetry (DSC). A cocrystal phase of DMC with one of the two trihydroxybenzenes could not be found, but a simple eutectic behavior was proven. Binary phase diagrams of all six systems were constructed from DSC measurements revealing distinct thermal behaviors: The CUR cocrystals both melt congruently, while the BDMC cocrystals show an incongruent melting behavior. Together with the eutectic DMC systems, we found three different types of binary phase behaviors for the CURD systems, which can serve as a basis for future crystallization-based purification of structurally similar CURDs.

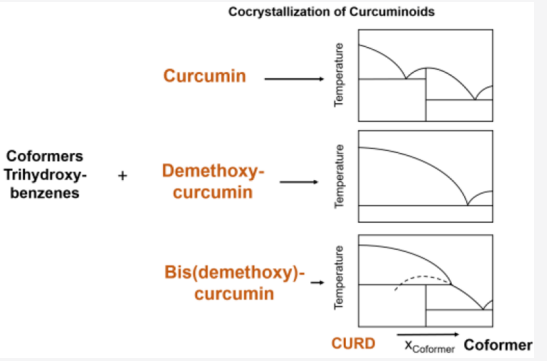

1. INTRODUCTION

Crystallization of two or multiple components in a certain stoichiometric ratio to form new multicomponent crystals, so-called cocrystals, is a promising approach to modify properties of materials.[1−4] Especially in the field of pharmaceuticals, cocrystals are of interest as they can influence solubilities, increase dissolution rates, and stabilize active pharmaceutical ingredients (APIs).[5−10] In addition, the control over these aforementioned physicochemical properties allows the utilization of cocrystallization for effective separation and purification of substances. For example, Urbanus et al.[11] used cocrystallization for the separation of a target compound from a model fermentation broth. Enantiospecific cocrystallization is beneficial in the separation of chiral compounds.[12,13] Different techniques can be applied to form cocrystals, including cocrystallization from a solution and the melt phase, and dry and liquid-assisted grinding.[14] Investigating multiple cocrystallization techniques is recommended as it is often found that one technique yields cocrystals where other means fail.[15−19] In this work, two techniques have been applied: liquid-assisted grinding and cocrystallization from the melt phase. To evaluate the outcomes of the cocrystallization experiments, the solid−liquid equilibria of the binary target component-coformer systems, the melt phase diagrams, are of particular interest.

Turmeric (Curcuma longa L.) originating in South and Southeast Asia has been used as a spice and in traditional medicine for centuries, e.g., for the treatment of wounds and ailments such as colds and arthritic disorders among others.[20] The main bioactive constituents of turmeric are the three structurally related curcuminoids (CURDs) curcumin (CUR), demethoxycurcumin (DMC), and bis(demethoxy)curcumin (BDMC). They differ only in the presence or absence of one or two methoxy groups (Figure 1). The main constituent CUR is known to exist in three polymorphic forms.[21] The thermodynamically stable form 1 crystallizes in the monoclinic space group $P2/n$. Form 2 and form 3 build an orthorhombic crystal lattice in space groups $Pca2_1$ and $Pcba$, respectively.

Received: January 28, 2022
Revised: March 30, 2022
Published: April 11, 2022

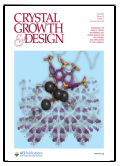

https://doi.org/10.1021/acs.cgd.2c00123
Cryst. Growth Des. 2022, 22, 3303−3310

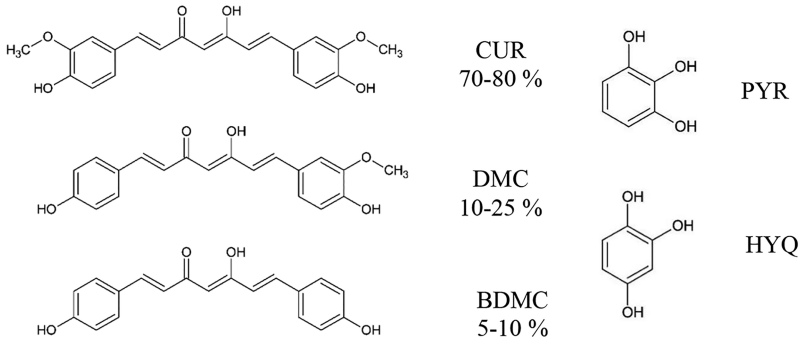

Figure 1. Molecular structures of the curcuminoids curcumin (CUR), demethoxycurcumin (DMC), and bis(demethoxy)curcumin (BDMC) (keto−enol form), and the hydroxybenzenes pyrogallol (PYR) and hydroxyquinol (HYQ). For the CURDs, their relative content in the plant extract is specified.[36,37]

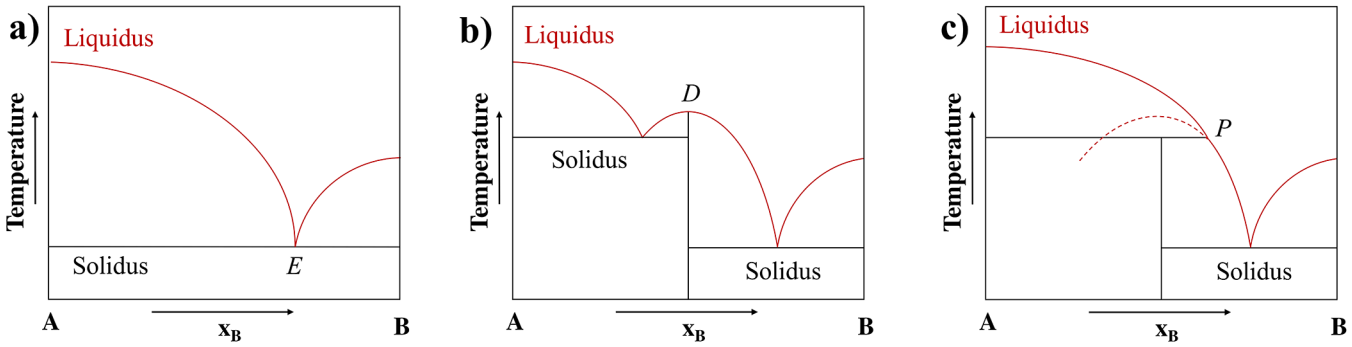

Figure 2. Different types of binary phase diagrams with complete immiscibility in the solid state, (a) eutectic system with eutectic invariant E, (b, c) cocrystal forming systems showing congruent and incongruent melting behavior with a dystectic (D) and peritectic (P) invariant, respectively (here with a 1:1 cocrystal stoichiometry). The vertical black line represents the fixed composition of the cocrystal single phase; marked black horizontal lines are solidus lines, and red lines represent liquidus lines.

Three solvates with 1,4-dioxane, methyl acetate, and dichloromethane and several cocrystals, e.g., with resorcinol, catechol, hydroquinone, pyrogallol, hydroxyquinol, and nicotinamide have been discovered to date.[22−26] For BDMC, only one crystal structure in the monoclinic space group $P2/c$ is known.[27] Besides that, six solvates with acetone, methanol, isopropanol, tetrahydrofuran, 1,4-dioxane, and dimethyl sulfoxide and two cocrystals with pyrogallol and hydroxyquinol were discovered.[27−29] So far, there are no crystal structure data available for DMC.

In the present study, the system of the curcuminoids was chosen for the investigation of their constituents' phase behavior in binary systems with two trihydroxybenzenes pyrogallol (PYR) and hydroxyquinol (HYQ) as coformers (Figure 1). Pyrogallol crystallizes in the monoclinic space group $P2_1/n$ and forms a tetarto hydrate in the tetragonal space group $P4_2/n$.[30] The crystal structure of HYQ has not yet been solved. The CURDs system is of particular interest because of its potential versatile health benefits. But still, crystallization-based separation of the three curcuminoids remains challenging due to their structural resemblance. CUR can be purified from the mixture using classical and nonclassical crystallization routes.[31−34] Purification and separation of CURDs from the remaining mother liquor can be carried out by chromatography.[31] Previous contributions (including our work) confirmed the presence of cocrystals of CUR and BDMC in a 1:1 molar composition with both trihydroxybenzenes.[25,26,29,35] To the best knowledge of the authors, this is the first time that binary mixtures of DMC with PYR and HYQ have been studied. Binary phase diagrams of all systems under investigation are constructed from experimental data and compared to calculated ones using the Schroeder−van Laar and Prigogine−Defay equation, respectively. The goal of this study is to investigate the phase behavior of the curcuminoids in binary systems and to gain insights into the possibilities of using cocrystallization as a possible crystallization-based separation technique for the CURDs.

2. BASIC NOTATIONS ON MELT PHASE EQUILIBRIA OF COCRYSTALS

The thermal phase behavior of a cocrystal as an intermediate compound of two components can be described by the binary melt phase diagram of the two constituents. Assuming complete immiscibility of the mixture components in the solid state, there are three types of binary melt phase diagrams showing the existence of solid and liquid phases depending on the temperature at a given pressure. For an arbitrary system of components A and B, these phase diagrams are schematically presented in Figure 2.

Figure 2a shows a eutectic system where the liquidus lines represent the melting temperature depression of A and B in the presence of the respective other component, which intersect at the eutectic temperature specifying the eutectic composition in the system (eutectic invariant E). Figure 2b,c represents systems where components A and B form an intermediate compound AB, that is, crystallized together in one new single phase with a fixed (here exemplarily equimolar) stoichiometry, a cocrystal. The melting behavior of such a cocrystal can be

https://doi.org/10.1021/acs.cgd.2c00123
Cryst. Growth Des. 2022, 22, 3303−3310

either congruent (Figure 2b) or incongruent (Figure 2c). The binary phase diagram of a congruent melting cocrystal is characterized by a so-called open maximum, the dystectic invariant D. In contrast, incongruent melting cocrystals decompose before melting at the peritectic temperature into a new solid phase (component A in Figure 2c) and a liquid phase with a composition different from the initial one (peritectic invariant P).[38−40] The liquidus line represents the thermodynamic equilibrium between the liquid and the corresponding solid phase and confines a single-phase liquid region from a two-phase solid and liquid section. By analogy, the solidus line segregates a section of solid phases at a lower temperature from a section of liquid and solid phases at higher temperatures.

Phase diagrams can be described mathematically using classical thermodynamic equilibrium equations.[39,41] Assuming ideal behavior and immiscibility in the solid state, the simplified Schroeder−van Laar equation (eq 1) can be used to describe the liquidus lines for a eutectic system of components $i = A, B$:[41,42]

$$\ln(x_i) = \frac{\Delta_F H_i}{R}\left(\frac{1}{T_{F,i}} - \frac{1}{T}\right) \quad (1)$$

where x_i is the mole fraction, $\Delta_F H_i$ the enthalpy of fusion, $T_{F,i}$ the melting temperature of component i, T is the actual temperature, and R is the universal gas constant. The so-called Prigogine−Defay equation (eq 2) describes the ideal melting behavior of a congruent melting cocrystal AB with a 1:1 molar composition:[43,44]

$$\ln(4x_{AB}(1 - x_{AB})) = \frac{\Delta_F H_{AB}}{R}\cdot\left(\frac{1}{T_{F,AB}} - \frac{1}{T}\right) \quad (2)$$

where x_{AB}, $\Delta_F H_{AB}$, and T_{AB} are the molar fraction, the enthalpy of fusion, and the melting temperature of the cocrystal AB.

3. EXPERIMENTAL SECTION

3.1. Materials. Curcumin (CUR) (CAS No. 458-37-7) and bis(demethoxy)curcumin (BDMC) (CAS No. 24939-16-0) with a purity higher than 98%, were obtained from TCI (Tokyo, Japan). Demethoxycurcumin (DMC) (CAS No. 22608-1-3) with a purity exceeding 98% was obtained from CfM Oskar Tropitzsch (Marktredwitz, Germany). Pyrogallol (PYR) (CAS No. 87-66-1) and hydroxyquinol (HYQ) (CAS No. 533-73-3) with a purity higher than 98% were purchased from Sigma-Aldrich (Germany). Solvents (acetone, ethanol, isopropanol) of HPLC grade were purchased from commercial suppliers. All materials were used as received without any further purification. Powder X-ray analyses confirmed CUR to be form 1 (Figure S1 (Supporting Information)). The diffractograms of BDMC and PYR match the reported ones for the unsolvated forms (Figures S2 and S3 (Supporting Information)). Since DMC was obtained as a partial amorphous substance, it was subjected to a liquid-assisted grinding treatment prior utilization to increase the crystallinity (see section 3.3).

3.2. Cocrystallization from the Melt Phase. Physical mixtures of BDMC and PYR in certain molar ratios were prepared by grinding the single components separately in a mortar, weighing them in a 5 mL glass vial, and gently mixing them by shaking the vial. Samples of 7.0 ± 0.5 mg were placed into a sealable aluminum crucible for thermal treatment in a DSC. The following temperature program was applied to produce molecular mixtures containing cocrystals from the eutectic melt: Mixtures were heated to 150 °C at a heating rate of 2 K·min^{-1}, kept there for 30 min to enable the formation of the cocrystal phase, and then cooled down to 25 °C at a cooling rate of 10 K·min^{-1}.

3.3. Liquid-Assisted Grinding (LAG). LAG experiments were performed on a Retsch MM400 mixing mill at a vibrational frequency of 30 Hz. Samples of 200 mg containing one curcuminoid and the respective coformer in the desired molar ratio and 40 μL of solvent together with one stainless steel ball of 10 mm diameter were put into a 10 mL screw-top grinding jar made of stainless steel and were ground for 90 min. Solvents were chosen so that no solvate formation of any involved substance could be expected. For the pretreatment of DMC, 200 mg of DMC was ground with 40 μL of acetone. After grinding, the jar was left open for solvent evaporation. Then, the samples were homogenized in a mortar and stored in a 5 mL glass vial for further analyses. Ethanol as solvent was used for experiments with CUR and BDMC; acetone and isopropanol were used for DMC.

3.4. Construction of Binary Phase Diagrams. DSC measurements of the cocrystallization products with mole fractions ranging from 0 to 1 with varying intervals were used to construct the binary phase diagrams. Samples were heated to 270 °C at a heating rate of 2 K·min^{-1}. The onset temperature of the first melting event and the peak temperature of the following melting events were taken for constructing the solidus and liquidus lines in the binary phase diagram.

3.5. Techniques. X-ray powder diffraction (PXRD) data were collected on an X'Pert Pro diffractometer (PANalytical GmbH, Kassel, Germany) using Cu−Kα radiation (λ = 1.5418 Å). Samples were prepared on a "zero-background" sample holder and scanned in a 2θ range of 3−40° with a step size of 0.017° and a counting time of 50 s per step at ambient temperature. Differential scanning calorimetry (DSC) analyses were performed on a Mettler Toledo DSC3 instrument. Samples of 4.0 ± 0.5 mg were put into a 40-μL aluminum crucible, sealed, and heated at a rate of 2 K·min^{-1}. Nitrogen was used as the purge gas at a flow rate of 30 mL·min^{-1}.

4. RESULTS AND DISCUSSION

4.1. Cocrystallization of Equimolar Mixtures of Curcuminoids with Hydroxybenzenes. First, cocrystallization experiments were carried out using LAG of equimolar mixtures of curcuminoids and hydroxybenzenes, except the system BDMC-PYR. It was shown that this binary mixture could only form cocrystals from the melt, and it was treated using the procedure described above (section 3.2).[29] For CUR and BDMC, the composition of the formed cocrystal phases was already confirmed to be equimolar.[25,26,29] The results of the DSC and PXRD analyses of all cocrystallization products are presented in Figures 3 and 4, respectively. No solvate formation during LAG could be detected by DSC. The DSC thermograms of the CUR− and BDMC−pyrogallol (Figure 3a) and the CUR− and BDMC−hydroxyquinol systems (Figure 3b) all show sharp and strong endothermic peaks at temperatures between the melting temperatures of the starting materials. These can be attributed to the melting of a cocrystal phase. However, from these measurements, it cannot be distinguished between congruent and incongruent melting behavior. The broad endothermic peak after the first peak of the BDMC systems can be regarded as a sign, though no proof for the incongruent melting behavior. Clarity could be obtained from DSC measurements of samples with different compositions of BDMC and the respective coformer.[29] Both DMC−pyrogallol and −hydroxyquinol systems exhibit a different behavior upon heating: A first endothermic event assigned to melting is observed below the melting points of the starting materials (PYR: 133.2 °C, HYQ: 140.8 °C, DMC: 175.7 °C) at 106.2 °C for PYR and 115.3 °C for HYQ as coformers (Figure 3a,b). These peaks are broad and small compared to those observed for the CUR and BDMC systems. In addition, they are followed by a very broad endothermic effect indicating a simple eutectic behavior. Further, the rather

https://doi.org/10.1021/acs.cgd.2c00123
Cryst. Growth Des. 2022, 22, 3303−3310

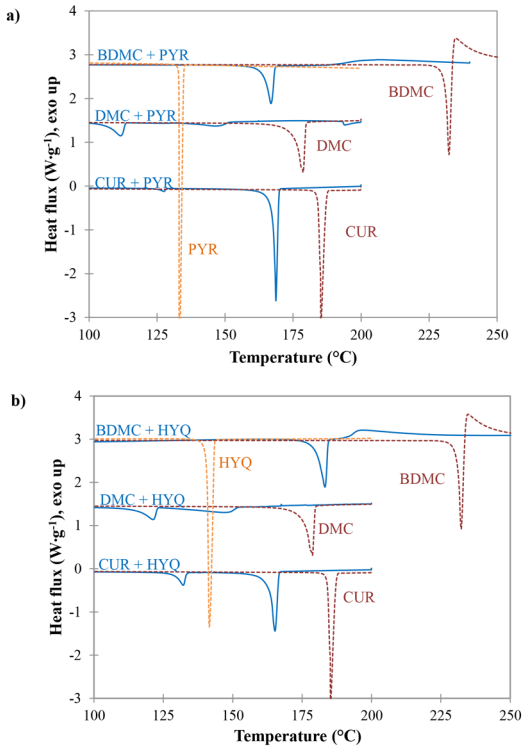

Figure 3. DSC thermograms of the cocrystallization outcomes of the curcuminoids CUR, DMC, and BDMC at a molar fraction of 0.5 with (a) PYR and (b) HYQ, measured at a heating rate of 2 K·min^{-1}. For comparison, DSC curves of the single CURD references and the PYR and HYQ coformers are shown in dashed red and orange lines, respectively.

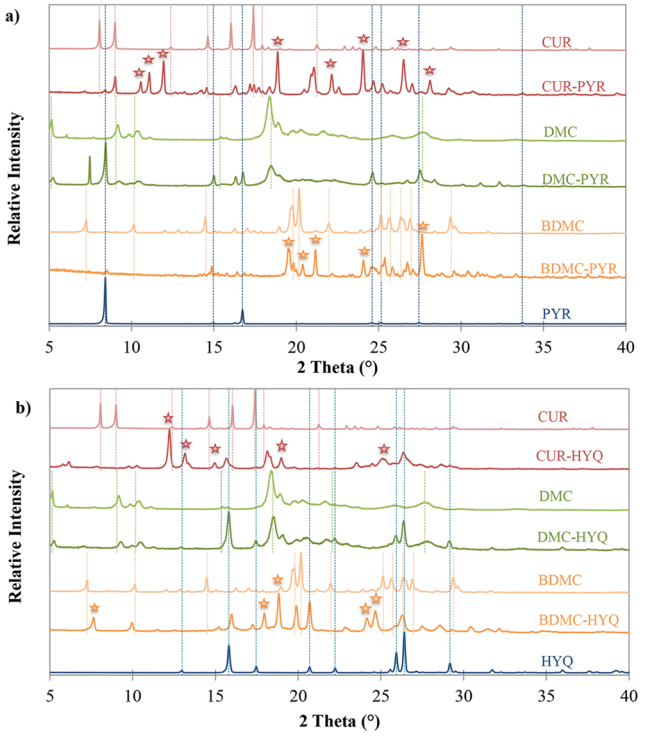

Figure 4. PXRD patterns of the cocrystallization outcomes of the curcuminoids CUR, DMC, and BDMC with (a) PYR and (b) HYQ, compared to the patterns of the single components; dashed lines indicate characteristic diffraction peaks of the starting materials; characteristic cocrystal diffraction peaks are asterisked. All samples were produced by LAG (except sample BDMC−PYR which was produced from the melt).

broad melting peak of DMC in Figure 3 can be attributed to its partial amorphous nature seen in Figure 4. DMC could not be purchased fully crystalline, and also attempts to recrystallize it were not completely successful up to now. But by LAG with acetone, the crystallinity could be increased significantly.

This assumption is confirmed by the analysis of the PXRD patterns in Figure 4. The binary systems of CUR and BDMC cocrystallized with PYR and HYQ (Figure 4a,b), respectively, reveal new diffraction peaks (marked with stars) providing evidence for the existence of a completely new phase. Moreover, the CUR-trihydroxybenzene diffractograms match the reported ones (Figures S4 and S5 (Supporting Information)).[25,26] In contrast, all diffraction peaks of the DMC−PYR (Figure 4a) and DMC−HYQ systems (Figure 4b) are correlated with the characteristic diffraction peaks of the single components which are indicated as dashed lines within the graphic. Thus, the formation of a potential solvate between DMC and the solvent used can be negated.

Very small eutectic melting peaks in the CUR−PYR and CUR−HYQ systems at temperatures of 127.5 and 132.2 °C in Figures 3a,b indicate incomplete phase transition. This is also noticeable in the respective PXRD patterns by the existence of characteristic diffraction peaks of CUR at 2θ of 9.0°, 14.6°, and 17.4° (Figure 4a).

4.2. Binary Phase Diagrams and Thermal Behavior. Binary phase diagrams (BPDs) of CUR−PYR and CUR−HYQ systems are shown in Figure 5. Experimental data are taken from the work of Wong et al.[25] Data measured in this study for x_{Coformer} = 0.5 are indicated by green triangles and fit excellently to the data of Wong et al. Both cocrystal forming systems exhibit a congruent melting behavior of the cocrystals CUR−PYR and CUR−HYQ with melting temperatures $T_{\text{F,cc}}$ of 165.7 and 165.0 °C, respectively. Hence, the Prigogine−Defay equation (eq 2) was used to calculate the ideal liquidus line for the cocrystal, and the simplified Schroeder−van Laar equation (eq 1) for the CUR, PYR, and HYQ liquidus lines to construct the ideal binary phase diagrams, shown as dashed lines in Figure 5. Both liquidus and resulting solidus curves deviate only slightly from the real melting behavior in the binary systems and thus roughly provide a good prediction of the phase diagrams. Each of the BPDs shown in Figure 5 can be divided into two sub-binary systems, for example, the CUR−PYR system into (1) the CUR−CUR•PYR and (2) the CUR•PYR−PYR subsystems, where each part is characterized by a eutectic invariant. The respective eutectic temperatures and corresponding eutectic compositions of the two subsystems of CUR with PYR and HYQ are compiled in Table T1 (Supporting Information).

In Figure 6, binary phase diagrams of the DMC−PYR and DMC−HYQ systems are presented. The pure reference substance of DMC is rare and as mentioned above not fully crystalline; that is why samples with only three different compositions (x_{DMC} = 0.25, 0.50, and 0.75) were produced to give a basic idea of how the binary phase diagram might look like. Under circumstances like these, using the Schroeder−van Laar equation (eq 1) to calculate the ideal binary phase diagram is supportive. Looking at the binary phase diagrams in Figure 6, it can be deduced that under the conditions applied in this study no cocrystal was formed between DMC and the

https://doi.org/10.1021/acs.cgd.2c00123
Cryst. Growth Des. 2022, 22, 3303−3310

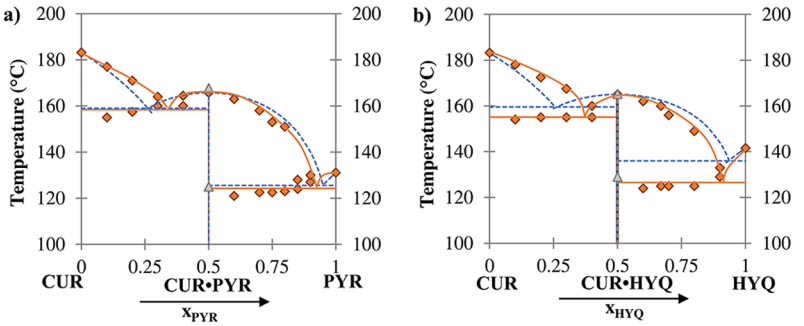

Figure 5. Binary phase diagrams of CUR and (a) PYR and (b) HYQ confirming cocrystal formation with a congruent melting behavior. Solid lines and diamonds represent the proposed BPD from experimental data from Wong et al.[25] (heating rate 10 K·min^{-1}, samples produced by rapid solvent removal), triangles are our own data (heating rate 2 K·min^{-1}). Dashed lines represent the calculated ideal BPD using the Prigogine–Defay and Schroeder–van Laar equations.

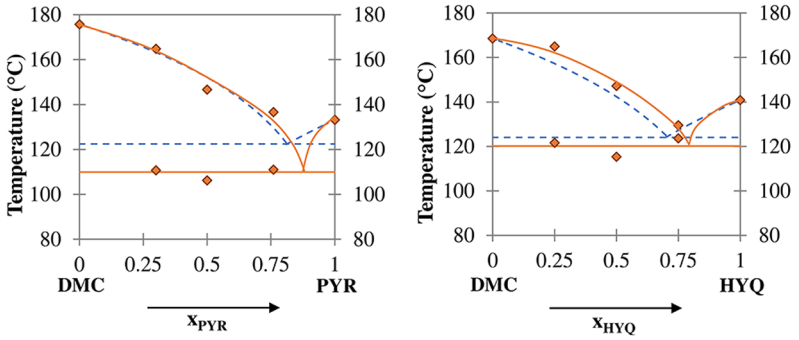

Figure 6. Binary phase diagrams of DMC and (a) PYR and (b) HYQ. Solid lines represent the proposed BPD from experimental data (heating rate 2 K·min^{-1}, samples produced by LAG), and dashed blue lines represent the calculated BPD using the simplified Schroeder–van Laar equation.

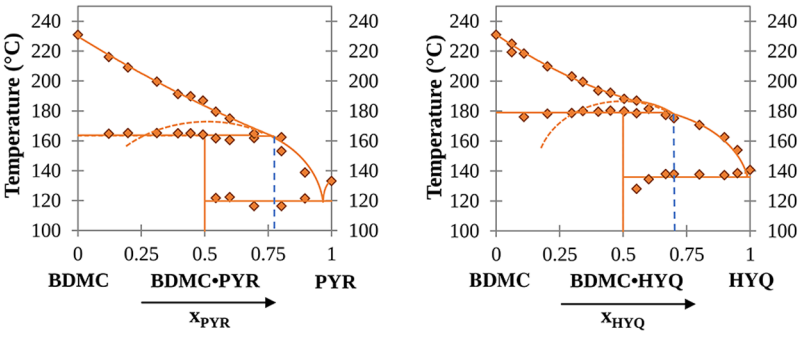

Figure 7. Binary phase diagrams of BDMC and (a) PYR and (b) HYQ; solid lines represent the proposed BPD from experimental data (heating rate 2 K·min^{-1}); vertical dotted blue lines illustrate the liquid phase composition after incongruent melting, PYR: samples produced from the melt, HYQ: samples produced by LAG.

two coformers used. In the DMC–PYR system (Figure 6a), there is only a small deviation between the calculated liquidus curve and the experimental data points on the DMC-rich side, indicating almost ideal behavior. The deviation on the PYR-rich side is supposed to be larger, which means that there is a higher melting point depression of PYR in the presence of DMC. The eutectic melting temperature of the real mixture is over 8 °C lower with a eutectic composition shifted to higher molar ratios of PYR compared to the ideal mixture. Consequently, an enhancement of the solubility can be expected at the eutectic composition that might be used for the enrichment of DMC as a potential target compound in a mother liquor containing all three CURDs. In addition, a higher solubility is beneficial for its application as an API.

The experimental data points for the DMC–HYQ system (Figure 6b) match quite well with the calculated liquidus and solidus curve, demonstrating the usefulness of the equation. Thus, it can be assumed that the system is almost ideal. Eutectic temperatures and compositions for both DMC–PYR and DMC–HYQ systems from Figure 6 are summarized in Table T2 (Supporting Information).

Most detailed data were acquired for the BDMC–PYR and BDMC–HYQ systems. The resulting binary melt phase diagrams are depicted in Figure 7. Interestingly, both systems show the formation of an incongruently melting 1:1 cocrystal phase characterized by a "hidden" maximum (dashed red line in Figure 7). By heating the equimolarly composed cocrystal, before melting, at the peritectic temperature (T_{peri}) a peritectic phase transition occurs where the cocrystal decomposes into

https://doi.org/10.1021/acs.cgd.2c00123
Cryst. Growth Des. 2022, 22, 3303–3310

solid BDMC and a liquid phase of defined composition. The latter is indicated in both BPDs by a vertical dotted blue line. Above T_{peri}, at equilibrium conditions, the cocrystal is not existent, and therefore, the hidden maximum is an indication of its metastable melting point.

Like the dystectic and eutectic phase transitions, the peritectic one is completely reversible. Cooling a melt with cocrystal stoichiometric composition to T_{peri} should first lead to crystallization of BDMC reaching and exceeding the respective liquidus line. Upon further cooling, at T_{peri}, a peritectic reaction between solid BDMC and the liquid phase takes place forming the cocrystal at the interface. Temperature-resolved PXRD analysis was applied to prove the incongruent melting behavior (Figure S6 (Supporting Information)). Nevertheless, the reformation of the cocrystal from the melt could not be observed clearly. Instead, the PXRD pattern of the recrystallized material showed BDMC and an amorphous background in the cocrystals fingerprint region (Figure S6 (Supporting Information)). Peritectic and eutectic temperatures with corresponding compositions of the BDMC−PYR and BDMC−HYQ systems are given in Table T3 (Supporting Information).

As to the knowledge of the authors, incongruently melting cocrystals are rarely reported. Most reported incongruent melting systems refer to inorganic compounds, such as salt hydrates and minerals.[45,46] However, we are not aware of another example of an incongruently melting 1:1 cocrystal, although the incongruent melting of 1:2 and 4:1 nicotinamide/(*R*)-mandelic acid cocrystals has been reported.[47]

An incongruent melting cocrystal can show an incongruent solubility behavior in certain solvents due to large differences in the solubility of the single components. Thus, the stability region of the BDMC•PYR/HYQ cocrystals might be different from the stability region of the corresponding CUR•PYR/HYQ cocrystals. Consequently, further investigations have to demonstrate its potential applicability in the cocrystallization-based separation of CUR and BDMC.

Whether a cocrystal melts congruently or incongruently depends on several factors, e.g., the relative thermodynamic stability of the cocrystal and its constituents. The melting temperatures of the CURDs increase in the order DMC < CUR < BDMC, while the melting enthalpies and entropies increase in the order BDMC < DMC < CUR. For a better overview, melting temperatures and corresponding melting enthalpies of CURDs, coformers, and CUR cocrystals are compiled in Table 1. Melting entropies were calculated using Gibb's equation at solid−liquid equilibrium. Regarding the coformers, they both have a lower melting temperature and enthalpy compared to the pure CURDs. Melting entropies for the CUR cocrystals are not directly accessible from that calculation. When melting, the cocrystal decomposes into the single components, which means the entropy term includes the contributions of both melting and decomposition. This, in fact, also applies to the measured heat of melting. However, the calculated entropies of both CUR cocrystals exceed the melting entropies of the single components. From that, it can be concluded that the cocrystals possess a higher degree of order in the solid state. This applies especially to the CUR•PYR cocrystal with an entropy value higher than the values of pure CUR and PYR combined.

Table 1. Thermal Data (Melting Temperature and Enthalpy) of CURDs, Coformers, and CUR Cocrystals from DSC Measurements and Melting Entropy Calculated from Thermal Data

sample	melting temp T_F (°C)	melting enthalpy ΔH_F (kJ·mol^{-1})	melting entropy ΔS_F (J·mol^{-1}·K^{-1})
CUR	184.4	52.1	113.8
DMC	175.7	46.5	103.6
BDMC	231.5	35.5	70.3
PYR	133.2	25.8	63.6
HYQ	140.8	29.2	70.7
CUR•PYR	168.7	82.6	189.3
CUR•HYQ	165.2	62.6	142.8

The BDMC molecules in the crystal lattice are very efficiently packed, resulting in a high melting point of the compound.[27] Intramolecular interactions are fewer due to the lower number of functional groups. It could be confirmed that to a small extent degradation starts before melting, which means that some intramolecular covalent bonds are more weakened by the thermal energy input than the intermolecular bonds.[29] Heffernan et al.[48] carried out electrostatic potential distribution analyses of a DMC molecule, which can be assumed to be a combination of CUR and BDMC as it involves a CUR-like phenyl ring on one side and a BDMC-like phenyl ring on the other side of the molecule. They could demonstrate that the methoxy group oxygen has the least negative electrostatic potential resulting in a lower propensity of forming H-bonding. Besides, the hydroxyl group proton connected to the phenyl ring possesses the most positive electrostatic potential. This potential is even higher in the absence of the methoxy group as in the BDMC molecule. This leads to the formation of stronger intermolecular H-bonding and further explains the high melting point of BMDC.[27] The melting temperatures of the CUR and BDMC cocrystals lie in between the melting temperatures of the single starting materials, which is in accordance with over 50% of the cocrystals found.[49] The CUR cocrystals both have a higher melting enthalpy than their single constituents, which is in accordance with their stability. For the peritectic phase transition enthalpy of the BDMC cocrystals, the enthalpy value of the BDMC•HYQ cocrystal (50 kJ·mol^{-1}) is higher than for the single components. For BDMC•PYR (38 kJ·mol^{-1}), it is in the same range as pure BDMC. This could be an indication of the proposed lower stability of this system since the cocrystal is only accessible from the melt phase at temperatures above the eutectic temperature so far. In addition, it could be shown from IR measurements that in this cocrystal BDMC is present in the less stable diketo form.[29] The reason for the incongruent melting behavior of the BDMC cocrystals is expected to be the exceedance of the intramolecular interaction energy of pure BDMC over the intramolecular interaction of the cocrystal at the peritectic temperature leading to the formation of solid BDMC. Besides, a large gap in melting temperatures of the involved components can promote an incongruent melting behavior.

5. CONCLUSIONS

Cocrystallization and the binary thermal phase behavior of the curcuminoids CUR, DMC, and BDMC with the trihydroxybenzenes pyrogallol and hydroxyquinol were investigated. CUR and BDMC were proven earlier to form cocrystals in a 1:1 stoichiometric ratio with the aforementioned coformers, but it is the first time that cocrystallization experiments of DMC are reported. Examination of two different cocrystalliza-

https://doi.org/10.1021/acs.cgd.2c00123
Cryst. Growth Des. 2022, 22, 3303−3310

tion techniques, namely, liquid-assisted grinding and cocrystallization from the melt phase, could not prove the existence of a cocrystal phase of DMC with one of the two trihydroxybenzenes. Instead, a simple eutectic behavior was proven for both systems under the conditions investigated in this study. DMC is rarely available and of poor initial crystallinity. Since there is no crystal structure solved until today, it can be assumed that there are only weak intermolecular interactions between the molecules, or the asymmetry of the DMC molecule hinders a periodical assembly. Also, the eutectic phase behavior and the near-ideality in the DMC−trihydroxybenzenes phase diagrams observed are indicative of rather low intermolecular interactions which might be too weak for cocrystal formation. However, this is not a proof that there are no cocrystals of DMC and the trihydroxybenzenes at all.

The melt phase diagrams, not yet known for four of the six binary systems studied, were determined and reveal a distinct phase behavior of the investigated systems: Whereas the CUR cocrystals melt congruently, the BDMC cocrystals disclose a rather rarely reported incongruent melting. In addition, DMC forms eutectic systems with the used trihydroxybenzenes. The three particular binary phase behaviors of the CURDs are potential starting points for upcoming investigations on the applicability of cocrystallization in terms of the crystallization-based separation of structurally very similar substances like the CURDs. The determination of the solubility behavior of the CURD-coformer systems to construct ternary phase diagrams will help to design separation experiments in future investigations.[50] Especially, a skillful choice of solvent will affect the solubility behavior in terms of congruency.

■ ASSOCIATED CONTENT

Supporting Information

The Supporting Information is available free of charge at https://pubs.acs.org/doi/10.1021/acs.cgd.2c00123.

Figure S1. PXRD of the CUR reference compared to calculated PXRD patterns of CUR polymorphs from the CSD database; Figure S2. PXRD of the BDMC reference compared to the calculated PXRD pattern of BDMC from the CSD database; Figure S3. PXRD of the PYR reference compared to calculated PXRD patterns of PYR anhydrate and tetarto hydrate from the CSD database; Figure S4. PXRD of the CUR−PYR cocrystallization product compared to calculated PXRD patterns of the CUR•PYR cocrystal from the CSD database. Figure S5. PXRD of the CUR−HYQ cocrystallization product compared to the measured PXRD pattern of the CUR•HYQ cocrystal from Wong et al.; Table T1. Cocrystal melting temperatures and eutectic temperatures with corresponding compositions of the CUR-cocrystal and cocrystal−coformer subsystems; Table T2. Eutectic temperatures with corresponding compositions of the DMC−PYR and DMC−HYQ systems from experimental data and calculated using the simplified Schroeder−van Laar equation; Figure S6. Temperature-resolved PXRD patterns of the BDMC•HYQ cocrystal; Table T3. Peritectic and eutectic temperatures with corresponding compositions of the BDMC−PYR and BDMC−HYQ systems from experimental data (PDF)

■ AUTHOR INFORMATION

Corresponding Author

Heike Lorenz − *Max Planck Institute for Dynamics of Complex Technical Systems, 39106 Magdeburg, Germany;* orcid.org/0000-0001-7608-0092; Email: lorenz@mpi-magdeburg.mpg.de

Authors

Steffi Wünsche − *Max Planck Institute for Dynamics of Complex Technical Systems, 39106 Magdeburg, Germany*

Andreas Seidel-Morgenstern − *Max Planck Institute for Dynamics of Complex Technical Systems, 39106 Magdeburg, Germany; Otto von Guericke University Magdeburg, 39106 Magdeburg, Germany*

Complete contact information is available at: https://pubs.acs.org/10.1021/acs.cgd.2c00123

Funding

Open access funded by Max Planck Society.

Notes

The authors declare no competing financial interest.

■ ACKNOWLEDGMENTS

The authors thank J. Kaufmann and S. Oberländer for performing DSC and PXRD measurements, respectively.

■ REFERENCES

(1) Stahly, G. P. Diversity in Single- and Multiple-Component Crystals. The Search for and Prevalence of Polymorphs and Cocrystals. *Cryst. Growth Des.* **2007**, *7* (6), 1007−1026.

(2) Aakeröy, C. B.; Sinha, A. S. Chapter 1. Co-crystals: Introduction and Scope. In *Co-crystals:Preparation, Characterization and Application*; Aakeröy, C. B., Sinha, A. S., Eds.; Royal Society of Chemistry, 2018; pp 1−32. DOI: 10.1039/9781788012874-00001.

(3) Desiraju, G. R. Crystal and co-crystal. *CrystEngComm* **2003**, *5* (82), 466.

(4) Bond, A. D. Inversion of the melting point alternation in n-alkyl carboxylic acids by co-crystallization with pyrazine. *CrystEngComm* **2006**, *8* (4), 333.

(5) Thakuria, R.; Delori, A.; Jones, W.; Lipert, M. P.; Roy, L.; Rodríguez-Hornedo, N. Pharmaceutical cocrystals and poorly soluble drugs. *International journal of pharmaceutics* **2013**, *453* (1), 101−125.

(6) Trask, A. V.; Motherwell, W. D. S.; Jones, W. Pharmaceutical Cocrystallization: Engineering a Remedy for Caffeine Hydration. *Cryst. Growth Des.* **2005**, *5* (3), 1013−1021.

(7) Good, D. J.; Rodríguez-Hornedo, N. Solubility Advantage of Pharmaceutical Cocrystals. *Cryst. Growth Des.* **2009**, *9* (5), 2252−2264.

(8) Fleischman, S. G.; Kuduva, S. S.; McMahon, J. A.; Moulton, B.; Bailey Walsh, R. D.; Rodríguez-Hornedo, N.; Zaworotko, M. J. Crystal Engineering of the Composition of Pharmaceutical Phases: Multiple-Component Crystalline Solids Involving Carbamazepine. *Cryst. Growth Des.* **2003**, *3* (6), 909−919.

(9) Karki, S.; Friščić, T.; Fábián, L.; Laity, P. R.; Day, G. M.; Jones, W. Improving Mechanical Properties of Crystalline Solids by Cocrystal Formation: New Compressible Forms of Paracetamol. *Adv. Mater.* **2009**, *21* (38−39), 3905−3909.

(10) Yan, D.; Delori, A.; Lloyd, G. O.; Friščić, T.; Day, G. M.; Jones, W.; Lu, J.; Wei, M.; Evans, D. G.; Duan, X. A cocrystal strategy to tune the luminescent properties of stilbene-type organic solid-state materials. *Angewandte Chemie (International ed. in English)* **2011**, *50* (52), 12483−12486.

(11) Urbanus, J.; Roelands, C. P. M.; Verdoes, D.; Jansens, P. J.; Ter Horst, J. H. Co-Crystallization as a Separation Technology: Controlling Product Concentrations by Co-Crystals. *Cryst. Growth Des.* **2010**, *10* (3), 1171−1179.

(12) Harmsen, B.; Leyssens, T. Dual-Drug Chiral Resolution: Enantiospecific Cocrystallization of (S)-Ibuprofen Using Levetiracetam. *Cryst. Growth Des.* **2018**, *18* (1), 441−448.
(13) Springuel, G.; Leyssens, T. Innovative Chiral Resolution Using Enantiospecific Co-Crystallization in Solution. *Cryst. Growth Des.* **2012**, *12* (7), 3374−3378.
(14) Chadwick, K. *Nucleation and Phase Relationships for Co-crystals*. Dissertation, University of Manchester, Manchester, 2008.
(15) Etter, M. C.; Frankenbach, G. M.; Bernstein, J. Solid-state nucleophilic aromatic substitution reaction of a carboxylic acid cocrystal. *Tetrahedron Lett.* **1989**, *30* (28), 3617−3620.
(16) Etter, M. C. Hydrogen bonds as design elements in organic chemistry. *J. Phys. Chem.* **1991**, *95* (12), 4601−4610.
(17) Etter, M. C.; Adsmond, D. A. The use of cocrystallization as a method of studying hydrogen bond preferences of 2-aminopyrimidine. *J. Chem. Soc., Chem. Commun.* **1990**, No. 8, 589.
(18) Etter, M. C.; Frankenbach, G. M. Hydrogen-bond directed cocrystallization as a tool for designing acentric organic solids. *Chem. Mater.* **1989**, *1* (1), 10−12.
(19) Etter, M. C.; Reutzel, S. M. Hydrogen bond directed cocrystallization and molecular recognition properties of acyclic imides. *J. Am. Chem. Soc.* **1991**, *113* (7), 2586−2598.
(20) DerMarderosian, A.; Beutler, J. A. *The Review of Natural Products: The Most Complete Source of Natural Product Information*, 7th ed.; Lippincott Williams and Wilkins, 2012.
(21) Sanphui, P.; Goud, N. R.; Khandavilli, U. B. R.; Bhanoth, S.; Nangia, A. New polymorphs of curcumin. *Chemical communications (Cambridge, England)* **2011**, *47* (17), 5013−5015.
(22) Wan, X.; Wu, S.; Wang, Y.; Gong, J. The formation mechanism of hollow spherulites and molecular conformation of curcumin and solvate. *CrystEngComm* **2020**, *22* (48), 8405−8411.
(23) Silva, T. de; Warner, I. M.; Fronczek, F. R. CCDC 1465072: Experimental Crystal Structure Determination. DOI: 10.5517/ccdc.csd.cc1l5jdp.
(24) Chava, S.; Gorantla, S. R. A.; Muppidi, V. K. Solid Forms of Curcumin and Derivatives thereof. Patent WO2015052568A3.
(25) Wong, S. N.; Hu, S.; Ng, W. W.; Xu, X.; Lai, K. L.; Lee, W. Y. T.; Chow, A. H. L.; Sun, C. C.; Chow, S. F. Cocrystallization of Curcumin with Benzenediols and Benzenetriols via Rapid Solvent Removal. *Cryst. Growth Des.* **2018**, *18* (9), 5534−5546.
(26) Sanphui, P.; Goud, N. R.; Khandavilli, U. B. R.; Nangia, A. Fast Dissolving Curcumin Cocrystals. *Cryst. Growth Des.* **2011**, *11* (9), 4135−4145.
(27) Yuan, L.; Horosanskaia, E.; Engelhardt, F.; Edelmann, F. T.; Couvrat, N.; Sanselme, M.; Cartigny, Y.; Coquerel, G.; Seidel-Morgenstern, A.; Lorenz, H. Solvate Formation of Bis(demethoxy)-curcumin: Crystal Structure Analyses and Stability Investigations. *Cryst. Growth Des.* **2019**, *19* (2), 854−867.
(28) Yuan, L.; Lorenz, H. Solvate Formation of Bis(demethoxy)-curcumin: Screening and Characterization. *Crystals* **2018**, *8* (11), 407.
(29) Wünsche, S.; Yuan, L.; Seidel-Morgenstern, A.; Lorenz, H. A Contribution to the Solid State Forms of Bis(demethoxy)curcumin: Co-Crystal Screening and Characterization. *Molecules (Basel, Switzerland)* **2021**, *26* (3), 720.
(30) Braun, D. E.; Bhardwaj, R. M.; Arlin, J.-B.; Florence, A. J.; Kahlenberg, V.; Griesser, U. J.; Tocher, D. A.; Price, S. L. Absorbing a Little Water: The Structural, Thermodynamic, and Kinetic Relationship between Pyrogallol and Its Tetarto-Hydrate. *Cryst. Growth Des.* **2013**, *13* (9), 4071−4083.
(31) Heffernan, C.; Ukrainczyk, M.; Gamidi, R. K.; Hodnett, B. K.; Rasmuson, Å. C. Extraction and Purification of Curcuminoids from Crude Curcumin by a Combination of Crystallization and Chromatography. *Org. Process Res. Dev.* **2017**, *21* (6), 821−826.
(32) Horosanskaia, E.; Yuan, L.; Seidel-Morgenstern, A.; Lorenz, H. Purification of Curcumin from Ternary Extract-Similar Mixtures of Curcuminoids in a Single Crystallization Step. *Crystals* **2020**, *10* (3), 206.
(33) Kumar, K. V.; Ramisetty, K. A.; Devi, K. R.; Krishna, G. R.; Heffernan, C.; Stewart, A. A.; Guo, J.; Gadipelli, S.; Brett, D. J. L.; Favvas, E. P.; Rasmuson, Å. C. Pure Curcumin Spherulites from Impure Solutions via Nonclassical Crystallization. *ACS omega* **2021**, *6* (37), 23884−23900.
(34) Ukrainczyk, M.; Hodnett, B. K.; Rasmuson, Å. C. Process Parameters in the Purification of Curcumin by Cooling Crystallization. *Org. Process Res. Dev.* **2016**, *20* (9), 1593−1602.
(35) Sathisaran, I.; Dalvi, S. V. Crystal Engineering of Curcumin with Salicylic Acid and Hydroxyquinol as Coformers. *Cryst. Growth Des.* **2017**, *17* (7), 3974−3988.
(36) Aggarwal, B. B.; Sundaram, C.; Malani, N.; Ichikawa, H. Curcumin: the Indian solid gold. *Advances in experimental medicine and biology* **2007**, *595*, 1−75.
(37) Lee, W.-H.; Loo, C.-Y.; Bebawy, M.; Luk, F.; Mason, R. S.; Rohanizadeh, R. Curcumin and its derivatives: their application in neuropharmacology and neuroscience in the 21st century. *Current neuropharmacology* **2013**, *11* (4), 338−378.
(38) Weingärtner, H. *Chemische Thermodynamik*; Springer eBook Collection Life Science and Basic Disciplines; Vieweg+Teubner Verlag, 2003. DOI: 10.1007/978-3-322-91221-3.
(39) Lorenz, H. Solubility and Solution Equilibria in Crystallization. In *Crystallization:Basic Concepts and Industrial Applications*, 1st ed.; Beckmann, W., Ed.; John Wiley & Sons Incorporated, 2013; pp 35−74.
(40) Yamashita, H.; Hirakura, Y.; Yuda, M.; Teramura, T.; Terada, K. Detection of cocrystal formation based on binary phase diagrams using thermal analysis. *Pharm. Res.* **2013**, *30* (1), 70−80.
(41) Rastogi, R. P. Thermodynamics of phase equilibria and phase diagrams. *J. Chem. Educ.* **1964**, *41* (8), 443.
(42) Coquerel, G. Review on the heterogeneous equilibria between condensed phases in binary systems of enantiomers. *Enantiomer* **2000**, *5* (5), 481−498.
(43) Prigogine, I.; Defay, R. *Chemical Thermodynamics*, 4th ed.; Longmans, 1967.
(44) Kolbe, B.; Gmehling, J.; Kleiber, M.; Rarey, J. *Chemical Thermodynamics for Process Simulation*, Second, completely revised and enlarged ed.; Wiley-VCH, 2019.
(45) Dalal, M. *A Textbook of Physical Chemistry*, 1st ed.; Dala Institute, 2018; *Vol. 1*.
(46) Polonka, J. *Incongruent melting and melt textured solidification process of* $Bi_2Sr_2CaCu_2O_8$. Dissertation, Iowa State University, Ames, 1993.
(47) Zhang, S.-W.; Harasimowicz, M. T.; de Villiers, M. M.; Yu, L. Cocrystals of nicotinamide and (R)-mandelic acid in many ratios with anomalous formation properties. *J. Am. Chem. Soc.* **2013**, *135* (50), 18981−18989.
(48) Heffernan, C.; Ukrainczyk, M.; Zeglinski, J.; Hodnett, B. K.; Rasmuson, Å. C. Influence of Structurally Related Impurities on the Crystal Nucleation of Curcumin. *Cryst. Growth Des.* **2018**, *18* (8), 4715−4723.
(49) Perlovich, G. L. Thermodynamic characteristics of cocrystal formation and melting points for rational design of pharmaceutical two-component systems. *CrystEngComm* **2015**, *17* (37), 7019−7028.
(50) Chiarella, R. A.; Davey, R. J.; Peterson, M. L. Making Co-Crystals The Utility of Ternary Phase Diagrams. *Cryst. Growth Des.* **2007**, *7* (7), 1223−1226.

https://doi.org/10.1021/acs.cgd.2c00123
Cryst. Growth Des. 2022, 22, 3303−3310